

锡在 Cu_6Sn_5 金属间化合物表面的润湿行为

李富祥, 王建斌, 叶长胜, 林巧力

(兰州理工大学, 省部共建有色金属先进加工与再利用国家重点实验室, 兰州, 730050)

摘要: 利用改良座滴法研究了高真空条件下熔融纯 Sn 在 350 ~ 450 °C 下分别与 Cu_6Sn_5 和 T2 纯铜的润湿行为. 结果表明, 表面镀金的金属间化合物基板在各试验温度下的润湿性均优于纯铜基板; 金属基板表面氧化膜对润湿性的影响不容忽视; 离子溅射后表面形成的金膜可以作为一种改善润湿性及控制界面 IMC 厚度的有效方法; 润湿性改善的机制为 Sn 与氧化膜的化学反应, 界面析出 IMC 或者 IMC 的溶解过程并非限制铺展的主要因素; 铺展过程表现出线性铺展规律, 可用反应产物控制模型对其进行描述, 计算得到 Sn/ Cu_6Sn_5 和 Sn/Cu 两体系的铺展激活能分别为 20.469 kJ/mol 和 22.270 kJ/mol.

关键词: 金属间化合物; 润湿性; 钎焊

中图分类号: TG 454

文献标识码: A

doi: 10.12073/j.hjxb.20190628001

0 序言

在电子封装领域, 鉴于 SnPb 钎料中 Pb 对人体及环境的危害性, 无铅钎料一直被倡导替代含铅钎料. 自 2006 年 RoHS 颁布以来, 市场上流行各种无铅锡基钎料. 虽然无铅锡基钎料强度和抗蠕变性能优于传统 Sn-Pb 共晶钎料^[1-3], 但润湿性不足导致其使用条件较为苛刻. 故对于钎料的推广使用而言, 如何改善润湿性首先要了解其相应的润湿机制^[4-6].

Sn-Cu 是典型的反应润湿体系, 在采用 Sn 基钎料钎焊铜件的过程中, 界面发生化学反应的同时常常伴有界面产物 (Cu_6Sn_5 , Cu_3Sn IMCs) 的析出. 其中 IMCs 的析出促进润湿的作用显而易见, 然而体系最终的润湿性能否参照反应润湿控制 (RPC) 模型^[7], 即反应产物决定最终润湿性, 还不得而知. Wedi 等人^[8]研究了 SnPb/Cu 体系的反应润湿, 通过调控 Pb 的含量, 来研究反应产物 IMC 对润湿性的影响, 其认为一旦系统达到润湿平衡, 即便是反应产物继续增加, 接触角恒为定值, 不再变化. 这似乎符合 RPC 模型的规律, 然而即便在同样的润湿体系中存在相同的界面反应产物, 被报道的接触角仍大相径庭^[9]. 也曾有学者采用润湿平衡法研究了 Sn 基钎料与 Sn-Cu IMCs 的润湿行为, 但鉴于此方

法不能保证较好的真空状态且往往需要配合使用钎剂, 不同活性强度的钎剂造成润湿性数据的差异显著, 例如 Wang 等人^[10]报道富锡钎料与 Cu 和 $\text{Cu}_6\text{Sn}_5/\text{Cu}_3\text{Sn}/\text{Cu}$ 展现出相接近的润湿时间, 而文献 [11] 报道纯锡与 Cu_6Sn_5 不润湿. 综上, 在金属与金属的润湿体系中, 界面析出的 IMC 与润湿性的耦合关系仍不明确.

通过选取 Sn/Cu 和 Sn/ Cu_6Sn_5 润湿行为与界面微观结构为主要研究对象, 探究界面 IMC 对润湿性的作用, 并揭示其中的润湿机制. 研究结果有望加深对钎焊过程中基本物理现象的认识.

1 试验方法

试验所用的材料为 99.99% 的纯锡和尺寸为 20 mm × 20 mm × 1 mm 的 T2 纯 Cu. IMC 基板通过热浸镀的方法获得. 具体工艺为在 400 °C、高真空的环境下, 将 T2 铜板浸泡于熔融的 Sn 液中浸镀 2 h, 并在 300 °C 下保温约 336 h 后, 机械打磨去除浸镀后基板表面的残存锡, 再用 4% 的硝酸酒精溶液进行腐蚀, 进一步去除 IMC 层上残留的锡. 所制得的 IMC 基板经表面抛光后, 采用离子溅射仪 (HM-ETD-2000C, 中国) 在真空下条件下镀金. 基板的表面状态采用 X 射线光电子能谱仪 (XPS, Thermo ESCALAB 250, USA) 进行表征.

润湿试验在高真空 ($\sim 10^{-4}$ Pa) 环境中进行. 当

收稿日期: 2019 - 06 - 28

基金项目: 国家自然科学基金资助项目 (51665031; 51465032)

润湿温度、真空度稳定后,由外部磁力推进杆将待融锡粒推置 Al_2O_3 滴落管开口处,并使其落至基板表面.为获取熔滴在基板表面润湿的清晰轮廓,采用 650 nm 波长的激光作为背光源,在相机镜头前配以此波长的滤光片来过滤炉内杂光,待融锡粒完全融化(即 $t=0$ s, t 为熔滴在基板表面等温润湿的时间),采用高分辨相机记录整个润湿铺展过程,对所获得图像信息利用数据分析终端计算接触角和接触半径.

润湿试验后,选取典型样品,将其沿横截面切开并抛光,用配备能谱仪(EDS)的 FEG 450 扫描电子显微镜(SEM, Quanta Feg-450, 荷兰)对界面三相线、微观结构及化学组分进行分析.

2 试验结果

图 1 为 IMC 基板纵截面的微观结构. IMC 基板以 Cu 为基体,表面由两层连续的 IMC 层构成.在润湿试验中与液相直接接触的 Cu_6Sn_5 层平均厚度约 45 μm , 底下 Cu_3Sn 层约 22 μm . 由于金属/金属润湿体系中的润湿性对基板表面初始状态十分敏感,润湿试验前基板表面的原始状态由 XPS 表征,如图 2 所示. 图 2a 和 2b 分别为电荷校正后的 Cu2p 和 Au4f 的特征峰,分别对应于 Cu 基板(上部分黑线)和离子溅射后的 IMC 基板. 对于 Cu 基板,由于 Cu_2O 和金属铜的结合能很接近,并不能直接通过 Cu2p ($\text{Cu}2p_{1/2}$ 和 $\text{Cu}2p_{3/2}$) 峰将其区分,但微弱的卫星峰(如图 2a 中黑色虚线矩形标记)表明基板表面呈氧化状态(即有 Cu_2O 膜). 图 2b 中显示,由于 Au4f 区域具有良好的分离自旋轨道组分约为 3.7 eV,表明 IMC 上的 Au 处于金属态,且 Au 薄膜的厚度约为 10 nm,在 Au 薄膜下并未检测到 Cu 或 Sn 的氧化物.

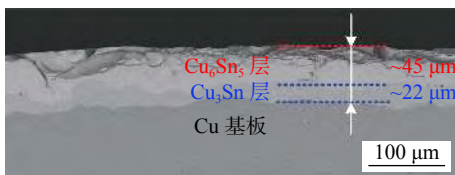


图 1 润湿试验前 IMC 基板界面结构

Fig. 1 Characterization of the IMC substrates before wetting test

图 3 为锡在铜基板表面及 IMC 基板表面润湿过程中接触角及归一化半径随时间变化的关系.从图中可以看出接触角跟半径都随时间呈单调变化,

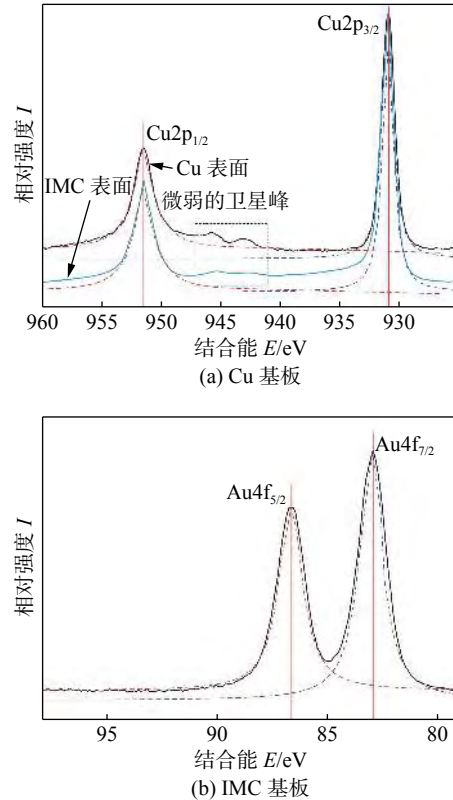


图 2 润湿试验前基板表面的 XPS 表征

Fig. 2 Characterization of the substrates by XPS. (a) Cu substrate; (b) IMC substrate

其中各个温度下,锡在 IMC 表面上的润湿性明显好于锡在铜表面的润湿性. 温度对 Sn/IMCs 的初始接触角有显著的影响,而对平衡接触角则影响不大;温度对 Sn/Cu 的初始接触角及平衡接触角的影响均不明显. 从归一化半径与时间的关系(图 2b),不难发现,3 个试验温度下,Sn/IMCs 的铺展速率均分别大于 Sn/Cu 的铺展速率,且前者在最低试验温度 350 $^{\circ}\text{C}$ 时的铺展速率比后者最高试验温度 450 $^{\circ}\text{C}$ 还要大得多.

润湿试验后,选取典型试样,对其横截面用 SEM 进行观察,如图 4 所示. 图 4a ~ 4b 和图 4c ~ 4d 分别对应于 400 $^{\circ}\text{C}$ 时 Sn/Cu 和 Sn/IMCs 的界面形貌. 图 4a, 4c 对应三相线附近的位置,图 4b, 4d 对应界面中心的位置. Sn/Cu 和 Sn/IMCs 两者的界面产物都分为上下两层,EDS 结果表明上层为 Cu_6Sn_5 , 下层为 Cu_3Sn , 且其平均厚度已在图中标记. 两个体系中 Cu_3Sn 均厚于 Cu_6Sn_5 , 且就 IMC 层的总厚度而言,Sn/Cu 体系界面中心处与三相线附近处无明显差异,Sn/IMCs 体系界面中心处却略厚于三相线附近处. 尽管 Sn/IMCs 具有更好的润湿性,但润湿试验前后界面 IMC 层的厚度变化并不显著,试

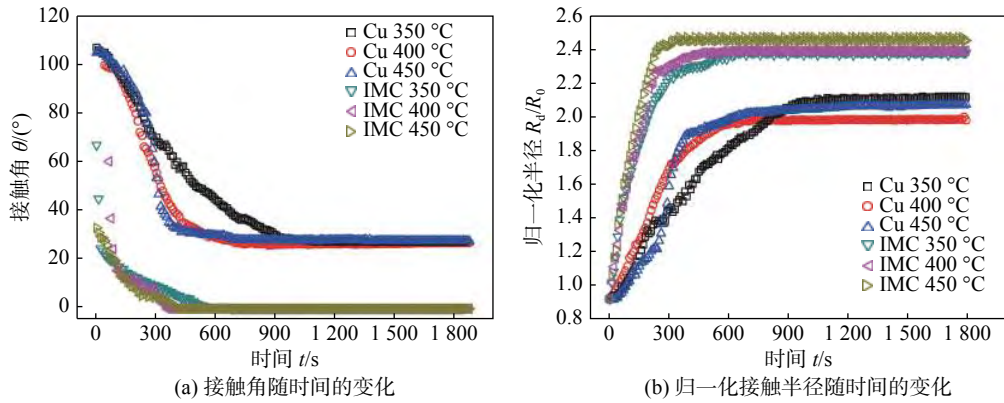


图 3 熔融纯 Sn 分别在纯 Cu 基板和 IMC 基板上接触角及归一化半径随时间的变化关系

Fig. 3 Variation of contact angles and normalized contact radius with time of molten pure Sn on the surfaces of Cu and IMC substrates. (a) contact angle v.s. *t*; (b) normalized contact radius v.s. *t*

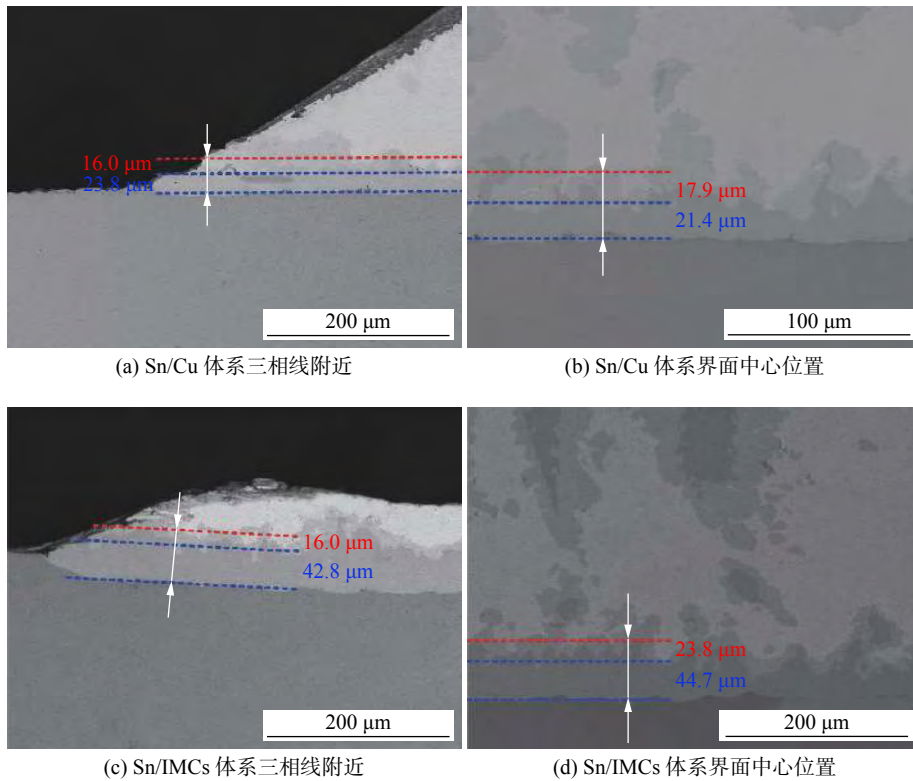


图 4 润湿试样界面 SEM 图

Fig. 4 Cross-sectional views of interfacial structure. (a) position close to triple line of Sn/Cu couple; (b) position at the central interface of Sn/Cu couple; (c) position close to triple line of Sn/IMC couple; (d) position at the central interface of Sn/IMC couple

验前 IMC 层的总厚度为 67 μm, 试验后界面中心处 IMC 层厚 68.5 μm, 三相线附近 IMC 层厚 58.8 μm, 这小范围的厚度变化说明了界面存在 IMC 的溶解, 具体表现为 Cu₃Sn 的增厚和 Cu₆Sn₅ 的变薄.

3 分析与讨论

按照反应产物决定润湿理论 (RPC 理论)^[8], 界面产物决定润湿性及润湿行为. 在 Sn/Cu 体系中, 倘若考虑到如下界面反应发生



Yost 等人^[12] 认为单位长度内体系的自由能可由下式描述

$$\frac{dG}{dr} = 2\pi r[\varepsilon + \sigma_{lv}^{S_n}(\cos \theta_d - \cos \theta_e)] \quad (2)$$

式中: *r* 为瞬时接触半径; $\sigma_{lv}^{S_n}$ 为 Sn 熔滴的表面张力; θ_d 为 Sn 熔滴的瞬时接触角; θ_e 为 Sn 熔滴的平衡接触角; ε 为反应中过剩自由能产生的铺展驱动力, 其值等于 $\rho_{Cu}l_{Cu}\Delta G/(xM_{Cu})$; ΔG 为 Cu_xSn_y 的

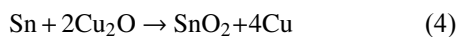
吉布斯形成自由能, Cu_6Sn_5 和 Cu_3Sn 的 ΔG 分别为 $-7\ 747.65 - 0.371 T$ (J/mol)^[12] 和 $-11\ 318.4 + 3.1 T$ (J/mol)^[13]; ρ_{Cu} 为 Cu 的密度; l_{Cu} 为反应层的厚度; M_{Cu} 为 Cu 的摩尔质量. 基于上式, 体系的铺展驱动力约为 $-3.3 \times 10^3 \sim -5.3 \times 10^3$ J/m², 与式 (2) 中表面张力引起的非平衡驱动力, 即 $\sigma_{\text{IV}}^{\text{Sn}}(\cos \theta_{\text{d}} - \cos \theta_{\text{e}})$ 相比 (约为 1 J/m²), 界面反应可能成为铺展的驱动力.

按照文献 [14-15] 报道, 界面先析出相为 Cu_6Sn_5 , 倘若铺展的行为由界面反应产物 Cu_6Sn_5 的析出决定, 那么 Cu_6Sn_5 的析出率或形核速率应与铺展速率相当. Cu_6Sn_5 的析出速率可以估算为^[16-17]

$$J = J_0 \exp \left[-\frac{16\pi\sigma_{\text{sl}}^3}{3kT(\Delta G_{\text{v}})^2} \left(\frac{\cos^3 \theta_{\text{n}} - 3\cos \theta_{\text{n}} + 2}{4} \right) \right] \quad (3)$$

式中: J_0 为表面形核的频率因子 (约为 $10^{31 \pm 1}$ /m²·s); σ_{sl} 为固液界面张力 (约为 0.05 ~ 0.15 J/m²)^[18-19]; k 为玻尔兹曼常数; θ_{n} 为形核与固相形成的接触角 (约为 23°)^[20]; ΔG_{v} 为形核驱动力 (约为 245 ~ 1 043 J/mol)^[18]. 假设形成 1 μm 厚的 Cu_6Sn_5 层, 形成的 Cu_6Sn_5 层扩展速率将在 10^5 m/s 数量级, 相比于三相线移动速率 ($\sim 10^{-6}$ m/s), 显然不受控于 Cu_6Sn_5 的析出.

按照整个动力学过程受限于其中最慢的一个环节, 假设三相线附近先发生如下反应



那么整个铺展过程有可能受限于反应 (4) 的动力学过程. 从图 3b 中的 R_{d}/R_0-t 曲线也可以看出近线性铺展的特征与反应控制铺展的特征相似. 值得注意的是 IMC 的润湿性对气氛中的氧十分敏感, 即使表面存在非常薄的金膜, 金膜随着加热过程中会固溶于 IMC 中, 进而形成 $(\text{Cu}, \text{Au})_6\text{Sn}_5$. 其中 IMC 基板润湿试验后的表面经 XPS 检测, 发现了 Cu_2O 的氧化峰印证了上述事实. 这就导致限制 Sn/Cu 和 Sn/IMCs 两个体系铺展的因素十分接近, 即受控于反应 (4). 其中 $\ln 1/t_{\text{e}}$ 与 $1/T$ 的 Arrhenius 曲线关系 (t_{e} 为达到铺展平衡所需的时间) 如图 5 所示, 可推导得到润湿激活能分别为 22.270 kJ/mol 和 20.469 kJ/mol, 两者相近的激活能表明铺展可能受限于同一机制. 反应 (4) 的反应吉布斯自由能如果按照表面相反应理论估算, 其值为体相反应自由能的 1/4, 那么也可以推导出铺展激活能与反应式

(4) 表面相反应的吉布斯自由能接近. 表明整个铺展过程受限于反应 (4) 的动力学过程.

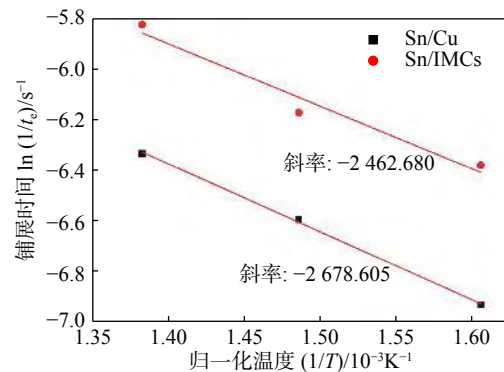


图 5 Sn/Cu 和 Sn/IMCs 体系的 Arrhenius 曲线图
Fig. 5 Arrhenius plot for Sn/Cu and Sn/IMCs systems

4 结论

(1) 在试验温度下, Sn 在 Cu_6Sn_5 表面的润湿性要好于 Sn/Cu 体系, 导致润湿性差异的主要原因来自于基板表面的氧化膜的影响, 故 RPC 模型不能用来预测此体系中的润湿性.

(2) Sn/Cu 和 Sn/IMCs 的润湿过程受限于锡与表面氧化膜的反应而非界面析出的金属间化合物, 铺展激活能为分别为 22.270 kJ/mol 和 20.469 kJ/mol.

参考文献

- [1] Cornelius B, Treivish S, Rosenthal Y, *et al.* The phenomenon of tinpest: a review[J]. *Microelectronics Reliability*, 2017, 79: 175-192.
- [2] 王慧, 薛松柏, 陈文学, 等. Ag, Al, Ga 对 Sn-9Zn 无铅钎料润湿性能的影响[J]. *焊接学报*, 2007, 28(8): 33-36.
Wang Hui, Xue Songbai, Chen Wenxue, *et al.* Effect of Ag, Al, Ga addition on wettability of Sn-9Zn lead-free solder[J]. *Transactions of the China Welding Institution*, 2007, 28(8): 33-36.
- [3] Cheng S, Huang C M, Pecht M. A review of lead-free solders for electronics applications[J]. *Microelectronics Reliability*, 2017, 75: 77-95.
- [4] Kang Yuqing, Shen Haoran, Fu Yang, *et al.* Microstructure evolution and mechanical properties of the Sip/Zn-Al composite joints by ultrasonic-assisted soldering in air[J]. *China Welding*, 2018, 17(2): 39-44.
- [5] 张亮, Tu K N, 孙磊, 等. Sn-0.3Ag-0.7Cu-xSb 无铅钎料润湿性[J]. *焊接学报*, 2015, 36(1): 59-62.
Zhang Liang, Tu K N, Sun Lei, *et al.* Wettability of Sn-0.3Ag-0.7Cu-xSb lead-free solders[J]. *Transactions of the China Welding Institution*, 2015, 36(1): 59-62.

- [6] 曾承宗, 林巧力, 曹睿, 等. 冷金属过渡下熔融铝合金在钢板上润湿铺展的数值模拟 [J]. 焊接学报, 2017, 38(3): 61 – 65.
Zeng Chengzong, Lin Qiaoli, Cao Rui, *et al.* Simulation of spreading of molten Al alloy on Q235 steel under the cold metal transfer condition[J]. Transactions of the China Welding Institution, 2017, 38(3): 61 – 65.
- [7] Eustathopoulos N, Nicholas M G, Drevet B. Wettability at high temperatures[M]. Oxford: Elsevier, 1999.
- [8] Wedi A, Baither D, Schmitz G. Contact angle and reactive wetting in the SnPb/Cu system[J]. Scripta Materialia, 2011, 64(7): 689 – 692.
- [9] Satyanarayana, Prabhu K N. Study of reactive wetting of Sn-0.7Cu and Sn-0.3Ag-0.7Cu lead free solders during solidification on nickel coated Al substrates[J]. International Journal of Chemical, Molecular, Nuclear, Materials and Metallurgical Engineering, 2013, 7: 25 – 28.
- [10] Wang H, Gao F, Ma X, *et al.* Reactive wetting of solders on Cu and $\text{Cu}_6\text{Sn}_5/\text{Cu}_3\text{Sn}/\text{Cu}$ substrates using wetting balance[J]. Scripta Materialia, 2006, 55(9): 823 – 826.
- [11] Hosking M, Yost F G. The mechanics of solder alloy wetting and spreading [M]. New York: Springer Science & Business Media, 2012.
- [12] Yost F G, Romig A D. Thermodynamics of wetting by liquid metals[M]. Pittsburgh: Materials Research Society, 1988.
- [13] Sobiech M, Krüger C, Welzel U, *et al.* Phase formation at the Sn/Cu interface during room temperature aging: Microstructural evolution, whiskering, and interface thermodynamics[J]. Journal of Materials Research, 2011, 26(12): 1482 – 1493.
- [14] Salleh M A A M, McDonald S D, Yasuda H, *et al.* Rapid Cu_6Sn_5 growth at liquid Sn/solid Cu interfaces[J]. Scripta Materialia, 2015, 100: 17 – 20.
- [15] Huang M L, Yang F, Zhao N, *et al.* In situ study on dissolution and growth mechanism of interfacial Cu_6Sn_5 in wetting reaction[J]. Materials Letters, 2015, 139: 42 – 45.
- [16] Volmer M, Weber A. Keimbildung in übersättigten Gebilden[J]. Zeitschrift für physikalische Chemie, 1926, 119(1): 277 – 301.
- [17] Bondy A. The spreading of liquid metals on solid surfaces[J]. Chemical Reviews, 1953(2): 417 – 458.
- [18] Bader S, Gust W, Hieber H. Rapid formation of intermetallic compounds interdiffusion in the Cu-Sn and Ni-Sn systems[J]. Acta Metallurgica Et Materialia, 1995, 43(1): 329 – 337.
- [19] Jena A K, Chaturvedi M C. Phase transformation in materials[M]. New Jersey: Prentice Hall, 1992.
- [20] Gagliano R A, Ghosh G, Fine M E. Nucleation kinetics of Cu_6Sn_5 by reaction of molten tin with a copper substrate[J]. Journal of Electronic Materials, 2002, 31(11): 1195 – 1202.

第一作者简介: 李富祥, 1992 年出生, 硕士; 主要从事金属的润湿性及界面结构研究; Email: lifuxiang163wy@163.com.
通信作者简介: 林巧力, 教授; Email: lqllinqiaoli@163.com.

(编辑: 曲畅)

thermal cycling were studied by in situ observation method using laser confocal microscope. The results show that the transformation from ferrite and pearlite to austenite is occurred while the heating temperature rises to 860 ~ 980 °C during thermal cycling. The austenite grain begins to grow obviously while the temperature reaches 1 100 °C. At the temperature range of 1 300 ~ 1 400 °C, the grain grows rapidly with the form of combining. During cooling process, when the temperature declines to 1 400 ~ 1 350 °C, the grain grows slowly with the form of grain boundary migrating. When the temperature decreases to 660 ~ 580 °C, the austenite transforms rapidly to bainite. The content of HAZ is mainly composed of bainite and ferrite. The size of austenite grain determines the maximum size of bainite. The formation, transformation and end temperature range of austenite and bainite decreases with the prolongation of the high temperature residence time. The content of proeutectoid ferrite decreases first and then increases, the content of bainite decreases, the polygonal ferrite disappears, and the cooling structure tends to be uniform and coarse. During the welding process, the choosing of appropriate high temperature residence time can increase the content of IAF in HAZ and improve the mechanical properties of the joints.

Key words: TiNbV microalloyed steel; welding heat cycle; welding heat affected zone; grain growth; phase transformation

Effect of ultrasonic power on microstructure and properties of 2219-T351 aluminum alloy friction stir welding joint

HE Diqu¹, HU Lei², ZHAO Zhifeng², LAI Ruilin² (1. Light Alloy Research Institute, Central South University, Changsha, 410083, China; 2. State Key Laboratory of High Performance Complex Manufacturing, Changsha, 410083, China). pp 23-28

Abstract: Aluminum alloy 2219-T351 plates were welded by friction stir welding and ultrasonic assisted friction stir welding with different power. The welding temperature and welding pressure were investigated. Microstructure, microhardness and mechanical properties of welds under different ultrasonic powers were analyzed. The microstructure and material fluidity of the weld with different ultrasonic power were researched. Experimental results showed that Ultrasonic energy can reduce the welding temperature and welding force. With the action of ultrasound, the microstructure of the weld is more uniform, and the fluidity of the bottom material is improved. There is more residual reinforcement phase in the weld zone. The microhardness, tensile strength and elongation of the welded joints are all

improved under ultrasonic. All the magnitudes reached the highest when adding 2.25 kW ultrasonic power. The highest tensile strength is 331 MPa, which can reach about 80% of the base metal.

Key words: friction stir welding; ultrasonic; welding temperature; microstructure; mechanical properties

Effect of different ultrasonic action stages on grain crystallization in TIG weld pool

CHEN Qihao^{1,2}, LIN Sanbao¹, YANG Chunli¹, FAN Chenglei¹, YAN Jiuchun¹ (1. State Key Laboratory of Advanced Welding and Joining, Harbin Institute of Technology, Harbin, 150001, China; 2. Jiangsu University of Science and Technology, Zhenjiang, 212003, China). pp 29-32,44

Abstract: The mechanism of the grain crystallization in TIG weld pool under different ultrasonic action is of great significance for optimizing the ultrasonic assisted TIG welding process. The grain distribution characteristics in the weld of aluminum-lithium alloy is analyzed by changing the ultrasonic action stage and style. The results showed that the edge of the weld is the broken columnar grain and the center of the weld is equiaxed grain with the ultrasonic action imposed after the arc is extinguished. The grain is equiaxed grain when the ultrasonic action is acted during whole welding process. Continuous ultrasonic action and transient ultrasonic action have different effects on crystal crystallization. Continuous ultrasonic action mainly promotes heterogeneous nucleation of grains in weld pool for the formation of equiaxed crystal. Transient ultrasonic action mainly broken dendrites. Ultrasonic refinement mechanism of the grain structure in the TIG weld of Al-Li alloy is directly related to the stage of ultrasonic action.

Key words: weld pool; ultrasonic action; grain refinement; aluminum lithium alloy

Wetting behavior of Cu₆Sn₅ IMC by molten Sn

LI Fuxiang, WANG Jianbin, YE Changsheng, LIN Qiaoli (State Key Laboratory of Advanced Processing and Recycling of Non-ferrous Metal, Lanzhou University of Technology, Lanzhou, 730050, China). pp 33-37

Abstract: Wetting behavior between the molten Sn and Cu₆Sn₅ and Cu under the temperature 350 ~ 450 °C was studied using the modified sessile drop method in the high vacuum. The results show that the IMCs substrates coated with a thin Au film have the better wettability than that of Sn/Cu system under the tested temperatures. The oxide film on the surface of metallic substrate is the key factor for wetting process. The thin passivation Au film on surface after ion-sputtering can be an effective method to improve the

wettability and control the IMC thickness at interface. The mechanism of wettability improvement is the reaction between Sn and the oxide film. The precipitated IMC at interface or the melt process of IMC is not the main factor for spreading. All spreading dynamics show the near-linear variation, which can be described by the reaction-limited spreading model. The calculated wetting activation energies are 20.469 kJ/mol and 22.270 kJ/mol for Sn/Cu₆Sn₅ and Sn/Cu, respectively.

Key words: intermetallic compounds(IMCs); wettability; soldering

Microstructure and mechanical properties of FSW joint of Mg/Al clad sheets CHEN Hongsheng¹, WANG Wenxian², CHEN Wei², ZHANG Tingting¹, LIU Runai¹, YANG Tao¹ (1. Taiyuan University of Technology, Taiyuan, 030024, China; 2. Shanxi Key Laboratory of Advanced Magnesium-based Materials, Taiyuan, 030024, China). pp 38-44

Abstract: The welding by one side and by both sides of Mg/Al clad sheets was conducted, and the microstructure and mechanical properties of Mg/Al clad sheets butt joints was tested using friction stir welding method. The results showed that with the increase of welding and rotating speed, the good weld surface appearance was obtained and no porosities and cracks were observed. The joint phase was mainly consisted of Mg₁₇Al₁₂, Mg₂Al₃ and MgAl phases, the size of grain is effectively refined and the dynamic recrystallization takes place. The formation of brittle intermetallic compounds is benefits to the formation of the recrystallization nucleus. Compared with joints with friction stir welding by one side, the joints of welding by both sides has much higher tensile strength and elongation due to the different distribution and quality of intermetallic compounds in welding joint. Inhibiting the formation of intermetallic compounds at the joints is beneficial to improve the performance of Mg/Al clad sheets of FSW joints.

Key words: Mg/Al clad sheets; friction stir welding; intermetallic compounds; tensile strength; elongation

Microstructure and mechanical properties of aluminum/AlSiNi/steel joint by induction brazing XUE Hongyu¹, LONG Weimin¹, JIU Yongtao¹, CHENG Zhan¹, HUANG Guoqin², ZHANG Fenglin³ (1. State Key Laboratory in Advanced Brazing Filler Metals and Technologies, Zhengzhou Research Institute of Mechanical Engineering Co., Ltd., Zhengzhou, 450001, China; 2. Huaqiao University, Xiamen, 361021, China; 3. Guangdong University of Technology, Guangzhou, 510006, China). pp 45-49

Abstract: The brazing performance of brazing filler

metals AlSi12 and AlSiNi was analyzed by means of wetting test and thermal analysis. The microstructure, fracture morphology, phase composition and mechanical property of aluminum/steel joints brazed by AlSi12 and AlSiNi were analyzed by means of SEM, EDS and tensile strength test. The results showed that the wettability of AlSiNi filler metal is better than that of AlSi12, but the melting regions slightly enlarged. The thickness of the intermetallic compound layer in the AlSiNi brazing joint is 8.1 μm, which is thinner and more uniformly distributed than that in the AlSi12 brazing joint. The Ni-containing intermetallic compounds in AlSiNi brazing joint have better plastic toughness and stronger bonding force with steel. As a result, aluminum/steel brazing joint with AlSiNi has higher tensile strength than that with the AlSi12 joint.

Key words: aluminum and steel brazing; Al-based filler metal; composition and morphology; mechanical property; intermetallic compound

Essence of the technology of filling keyhole based on resistance welding DENG Lipeng^{1,2}, KE Liming², LIU Jinhe¹ (1. Northwestern Polytechnical University, Xi'an, 710072, China; 2. Nanchang Hangkong University, Nanchang, 330063, China). pp 50-53

Abstract: The technology of filling keyhole based on resistance welding (FKBRW) is a new filling technology for friction stir welding (FSW) keyhole, which can not only achieve the purpose of removing the keyhole but also has a positive effect on the load bearing capacity of the FSW joint. For studying the mechanism of FKBRW, the keyholes of 2024-T4 aluminum alloy friction stir spot welding of 1.5 mm + 1.5 mm were filled on a three-phase secondary rectification resistance spot welding machine for test equipment, and a device monitoring the filling force dynamic behavior was built up. The results showed that there exists two bonding forms between the plug and wall of keyhole. The melting connection zone is in the middle of the joints, and the solid phase connection zone is on the both upper and bottom of the joints. The FKBRW technology is a kind of composite welding process that the filling force from upper electrode presses the plug into the keyhole, and the plug goes through the process of softening and pushing and metallurgical combines fully with the wall of keyhole in the last time.

Key words: friction stir welding; resistance welding; keyhole; aluminum alloy; technology of FKBRW

Tungsten/steel vacuum diffusion bonding using Co/Ni composite interlayer YANG Zonghui^{1,2}, SHEN Yifu³, CHU Yajie^{1,2}, CHENG Jialin^{1,2}, LI Xiaoquan^{1,2} (1. NanJing